Angular Velocity Bounds via Light Curve Glint Duration

Joanna C. Hinks* and John L. Crassidis†

The time duration of specular glint events within a light curve is related to the angular velocity of the reflecting space object. Upper and lower bounds on the magnitude of the observable part of angular velocity can be derived with some reasonable assumptions. The proposed method is independent of object shape or signal periodicity, and only loosely dependent on the choice of mathematical reflection model. This technique may be valuable in detecting when the overall spin rate of an object has changed, or in determining that a spacecraft that nominally has a fixed attitude is undergoing an attitude maneuver.

I. Introduction

A major research topic in recent years has been space situational awareness (SSA), which is concerned with the identification and tracking of all space objects (SOs) in orbit around Earth. This task faces many challenges, one of the greatest of which is inadequate data due to the limited number of available sensors. Consequently, many research efforts focus on extracting as much information as possible from the data. Of particular interest are techniques which determine or constrain the SO's attitude or angular velocity. These quantities may help in such tasks as SO identification or anomaly detection. One commonly available observation that depends strongly on attitude and angular velocity is the history of total reflected sunlight, or light curve.

Light curves have historically been used to investigate SOs in two ways: as part of a shape-model-based approach, or using model-independent techniques that focus predominantly on signal characteristics. Model-based approaches require a geometric model of the shape of the reflecting object, as in Refs. 1–4. Filters or other estimators can calculate the expected brightness sunlight reflected from a particular shape and compare those values to the observed light curve. Quantities such as attitude, angular rate, and surface material properties can be estimated. In the absence of reliable or sufficiently detailed models, however, model-based approaches may perform very poorly.

Signal-based approaches, in contrast, analyze the behavior of the observed light curve without making assumptions about the shape of the SO. Thus they may be very useful in cases where the shape is not well-known *a priori*. Model independence comes at a cost, however: a significant reduction in the types or precision of quantities that can be estimated.

One example of a signal-based approach is the use of simultaneous observations at multiple wavelengths to estimate surface materials.[5,6] One large family of signal-based algorithms exploits frequency content to spin rate, and in some cases, spin axis. These algorithms include, but are not limited to, Fourier analysis,[7–9] wavelet analysis,[5,6] and approaches based on feature periodicity (especially specular glint periodicity).[10,11] While such methods perform well for tumbling or spin-stabilized objects, they cannot be applied to signals that do not exhibit periodic behavior — such as three-axis-stabilized, geostationary objects. Furthermore, shape symmetries may cause the observed frequencies to be greater than the physical frequencies.

This paper presents proposes an algorithm that does not rely on mulispectral data or on frequency content. It analyzes the time duration (width) of individual specular glint events, and relates that value to SO angular rate. Reference 12 previously studied the angular extent of specular glints (as observed via duration or their spatial range of visiblity on Earth). However, that source emphasized the relationship of glint size to facet angle and surface properties, and did not rigorously develop the connection to angular rate.

*Postdoctoral Assistant, Department of Mechanical & Aerospace Engineering, University at Buffalo, State University of New York, Amherst, NY, 14260-4400. Email: jchinks@buffalo.edu. Member AIAA.

†CUBRC Professor in Space Situational Awareness, Department of Mechanical & Aerospace Engineering, University at Buffalo, State University of New York, Amherst, NY, 14260-4400. Email: johnc@buffalo.edu. Fellow AIAA.

The major weakness of this paper's algorithm is that it is imprecise; rather than giving a specific estimate of angular rate it merely provides upper and lower bounds on the observable component of that quantity. Even such limited information may prove valuable, however. One could detect unexpected attitude motion, identify changes in overall angular rate, or obtain a rough angular rate estimate that can be used to initialize a filter.

The remainder of this paper is organized as follows: Section II defines the problem geometry and derives the relationship between angular velocity and a quantity herein called "glint rate". In Section III, the relationship between glint rate and the light curve signal (specifically glint duration) is developed. Section IV addresses the role played by uncertainties in real applications and suggests some implementation guidelines. The algorithms are applied to three different data sets in Section V, and the results are discussed. Section VI draws some conclusions.

II. Glint Geometry and Rate

A. Scenario Configuration and Definitions

The goal of this paper is to derive bounds on the angular velocity $\boldsymbol{\omega}$, which describes the rotation of the space object's body-fixed B frame relative to the inertial I frame. At any given time, the two frames are related by tje attitude matrix A_{true}, such that the representations of any vector $\mathbf{v}$ in the I and B frames are related by $\mathbf{v}^B = A_{\text{true}}\mathbf{v}^I$.

It is common to distinguish between *synodic* angular rate and *sidereal* angular rate. The desired $\boldsymbol{\omega}$ is the sidereal angular rate; it is independent of the observer and describes only the physical relative motion of the two frames. The synodic angular rate is the name given to the apparent angular rate determined from the periodicity of a light curve; it additionally depends on the observer location and the relative motion of the Sun, SO, and observer.

This paper's techniques are independent of the particular shape of the reflecting space object. They do, however, require that the "glint conditions" are met: Namely, that the object includes some sufficiently large flat surface with surface normal vector $\mathbf{u}_n$ off of which sunlight reflects in a mirrorlike fashion. The object (or at least the currently glinting portion of it) is assumed to be a rigid body, and the surface normal vector is assumed to be constant in the body-fixed B frame (written as $\mathbf{u}_n^B$).

The inertial positions of the SO, Sun, and observer are given by the vectors $\mathbf{R}_{\text{SO}}$, $\mathbf{R}_{\text{sun}}$ and $\mathbf{R}_{\text{obs}}$, respectively. These vectors, and their derivatives, are assumed to be known and available. For the present application, it is most convenient to work in a coordinate system centered on the SO. In such a system, the relative positions of the Sun and the observer are given by $\mathbf{r}_{\text{sun}} = \mathbf{R}_{\text{sun}} - \mathbf{R}_{\text{SO}}$ and $\mathbf{r}_{\text{obs}} = \mathbf{R}_{\text{obs}} - \mathbf{R}_{\text{SO}}$. The corresponding line of sight (LOS) unit vectors are $\mathbf{u}_{\text{obs}}$ and $\mathbf{u}_{\text{sun}}$. Glints occur when any of the SO's facet normal vectors $\mathbf{u}_n$ gets very close to the "specular direction". The specular direction is aligned with the unit half-vector $\mathbf{u}_h$, which bisects the angle between $\mathbf{u}_{\text{obs}}$ and $\mathbf{u}_{\text{sun}}$:

$$\mathbf{u}_h = \frac{\mathbf{u}_{\text{obs}} + \mathbf{u}_{\text{sun}}}{\|\mathbf{u}_{\text{obs}} + \mathbf{u}_{\text{sun}}\|} \tag{1}$$

Another name for $\mathbf{u}_h$ is the phase angle bisector, because this vector bisects the Sun-SO-observer "phase angle". Figure 1 illustrates the surface basis vectors and LOS vectors that enter the light curve glint calculations.

Closeness to the glint direction (where $\mathbf{u}_n$ and $\mathbf{u}_h$ are aligned) is described by the angle θ between these two unit vectors. For this paper's purposes, a *full* glint is defined as one for which θ reaches 0. Practically speaking, most light curve glints are at best mostly full. Recall that the angle θ is related to the dot product between the two vectors by

$$\cos\theta = \mathbf{u}_h \cdot \mathbf{u}_n \tag{2}$$

B. Glint Rate

The duration of a glint event is determined by how quickly the angle θ approaches a value near zero and then increases. This glint rate, $\dot{\theta}$, depends on the rates of change of both $\mathbf{u}_n$ and $\mathbf{u}_h$ in the inertial frame. Note that the glint rate $\dot{\theta}$ is not to be confused with the frequency at which glints occur in a periodic light curve. The rate of change of $\mathbf{u}_n$ is related to the angular velocity of the B frame relative to the I frame, whereas the rate of change of $\mathbf{u}_h$ depends on the relative motion of the Sun, SO, and observer. An equation that

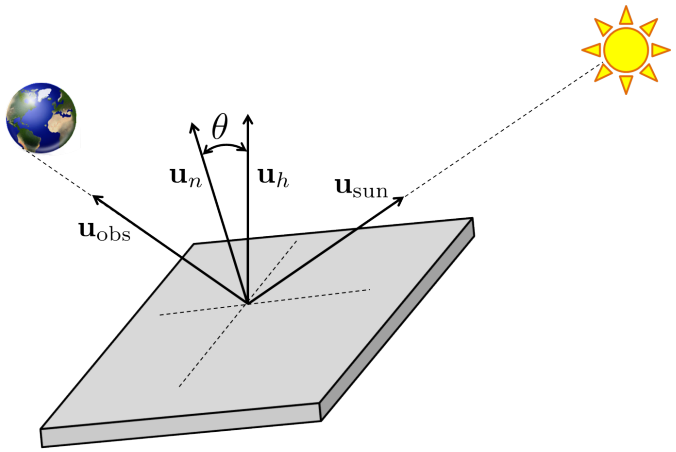

Figure 1. Reflection Geometry

describes the contributions from each of these sources can be derived as follows. Unless otherwise specified, derivatives are taken with respect to the inertial (I) frame.

Start by applying the product rule to the dot product $(\mathbf{u}_h \cdot \mathbf{u}_n)$:

$$\frac{{}^I d}{dt}(\mathbf{u}_h \cdot \mathbf{u}_n) = \left(\frac{{}^I d}{dt}\mathbf{u}_h\right) \cdot \mathbf{u}_n + \mathbf{u}_h \cdot \left(\frac{{}^I d}{dt}\mathbf{u}_n\right) \tag{3}$$

Equation (3) includes two unit vector derivatives. When taking the derivative of a unit vector, which may rotate but not stretch, it is necessary to explicitly include the normalization. Suppose an arbitrary unit vector $\mathbf{u}$ is defined as:

$$\mathbf{u} = \frac{\mathbf{v}}{\|\mathbf{v}\|} \tag{4}$$

The derivative of $\mathbf{u}$ is then given by:

$$\frac{d}{dt}\mathbf{u} = \frac{\left(\mathrm{I} - \mathbf{u}\mathbf{u}^{\mathrm{T}}\right)}{\|\mathbf{v}\|}\frac{d}{dt}\mathbf{v} \tag{5}$$

Applying Eq. (5) to the unit vector $\mathbf{u}_h$ as defined in Eq. (1) gives:

$$\frac{{}^I d}{dt}\mathbf{u}_h = \frac{\left(\mathrm{I} - \mathbf{u}_h\mathbf{u}_h^{\mathrm{T}}\right)}{\|\mathbf{u}_{\text{obs}} + \mathbf{u}_{\text{sun}}\|}\left(\frac{{}^I d}{dt}\mathbf{u}_{\text{obs}} + \frac{{}^I d}{dt}\mathbf{u}_{\text{sun}}\right) \tag{6}$$

The derivatives of $\mathbf{u}_{\text{obs}}$ and $\mathbf{u}_{\text{sun}}$ are in turn given by

$$\frac{{}^I d}{dt}\mathbf{u}_{\text{obs}} = \frac{\left(\mathrm{I} - \mathbf{u}_{\text{obs}}\mathbf{u}_{\text{obs}}^{\mathrm{T}}\right)}{\|\mathbf{r}_{\text{obs}}\|}\frac{{}^I d}{dt}\mathbf{r}_{\text{obs}} = \frac{\left(\mathrm{I} - \mathbf{u}_{\text{obs}}\mathbf{u}_{\text{obs}}^{\mathrm{T}}\right)}{\|\mathbf{r}_{\text{obs}}\|}\left(\mathbf{V}_{\text{obs}} - \mathbf{V}_{\text{SO}}\right) \tag{7a}$$

$$\frac{{}^I d}{dt}\mathbf{u}_{\text{sun}} = \frac{\left(\mathrm{I} - \mathbf{u}_{\text{sun}}\mathbf{u}_{\text{sun}}^{\mathrm{T}}\right)}{\|\mathbf{r}_{\text{sun}}\|}\frac{{}^I d}{dt}\mathbf{r}_{\text{sun}} = \frac{\left(\mathrm{I} - \mathbf{u}_{\text{sun}}\mathbf{u}_{\text{sun}}^{\mathrm{T}}\right)}{\|\mathbf{r}_{\text{sun}}\|}\left(\mathbf{V}_{\text{sun}} - \mathbf{V}_{\text{SO}}\right) \tag{7b}$$

Returning to Eq. (3), the derivative of $\mathbf{u}_n$ in the I frame is found by applying the transport theorem. The body-frame derivative of the facet normal vector is zero, so only the cross product term remains:

$$\frac{{}^I d}{dt}\mathbf{u}_n = \frac{{}^B d}{dt}\mathbf{u}_n + \boldsymbol{\omega} \times \mathbf{u}_n = \boldsymbol{\omega} \times \mathbf{u}_n \tag{8}$$

Substituting Eq. (8) into Eq. (3) yields:

$$\begin{aligned}\frac{{}^I d}{dt}(\mathbf{u}_h \cdot \mathbf{u}_n) &= \left(\frac{{}^I d}{dt}\mathbf{u}_h\right) \cdot \mathbf{u}_n + \mathbf{u}_h \cdot (\boldsymbol{\omega} \times \mathbf{u}_n) \\ &= \left(\frac{{}^I d}{dt}\mathbf{u}_h\right) \cdot \mathbf{u}_n + \boldsymbol{\omega} \cdot (\mathbf{u}_n \times \mathbf{u}_h)\end{aligned} \tag{9}$$

The second form of the equation uses an equivalent form of the scalar triple product. Also, note that $\frac{^I d}{dt}\mathbf{u}_h$ could be written in terms of known position and velocity vectors using Eqs. (6)-(7). It has been left in its original form here for conciseness.

Next, decompose the facet normal $\mathbf{u}_n$ into a component parallel to $\mathbf{u}_h$ and a component orthogonal to $\mathbf{u}_h$:

$$\mathbf{u}_n = \cos\theta \mathbf{u}_h + \sin\theta \mathbf{u}_p \tag{10}$$

In Eq. (10), the vector $\mathbf{u}_p$ is a unit vector that lies in the direction of the projection of $\mathbf{u}_n$ onto the plane orthogonal to $\mathbf{u}_h$. For purposes of this algorithm, it is a mathematical construct that does not need to be explicitly computed.

Substitute Eq. (10) into Eq. (9) and simplify. The simplification exploits the fact that the derivative of a unit vector is orthogonal to the vector itself: $\dot{\mathbf{u}} \cdot \mathbf{u} = 0$.

$$\begin{aligned}\frac{^I d}{dt}\left(\mathbf{u}_h \cdot \mathbf{u}_n\right) &= \left(\frac{^I d}{dt}\mathbf{u}_h\right) \cdot \left(\cos\theta \mathbf{u}_h + \sin\theta \mathbf{u}_p\right) + \boldsymbol{\omega} \cdot \left[\left(\cos\theta \mathbf{u}_h + \sin\theta \mathbf{u}_p\right) \times \mathbf{u}_h\right] \\ &= \sin\theta \left[\left(\frac{^I d}{dt}\mathbf{u}_h\right) \cdot \mathbf{u}_p\right] + \sin\theta \left[\boldsymbol{\omega} \cdot \left(\mathbf{u}_p \times \mathbf{u}_h\right)\right]\end{aligned} \tag{11}$$

An alternative form of this derivative can be found by differentiating Eq. (2):

$$\frac{^I d}{dt}\left(\mathbf{u}_h \cdot \mathbf{u}_n\right) = \frac{^I d}{dt}\left(\cos\theta\right) = -\dot{\theta}\sin\theta \tag{12}$$

Set Eqs. (11) and (12) equal and cancel the common $\sin\theta$ term to obtain

$$\dot{\theta} = -\left(\frac{^I d}{dt}\mathbf{u}_h\right) \cdot \mathbf{u}_p - \boldsymbol{\omega} \cdot \left(\mathbf{u}_p \times \mathbf{u}_h\right) \tag{13}$$

Finally, rearrange Eq. (13) to isolate the term with $\boldsymbol{\omega}$:

$$\dot{\theta} + \left(\frac{^I d}{dt}\mathbf{u}_h\right) \cdot \mathbf{u}_p = \boldsymbol{\omega} \cdot \left(\mathbf{u}_h \times \mathbf{u}_p\right) \tag{14}$$

Equation (14) would be most useful if the attitude (and thus $\mathbf{u}_p$) were known. In the absence of attitude knowledge, however, it is still possible to use the form of the equation to bound the magnitude of the angular velocity. The unit vectors $\mathbf{u}_h$ and $\mathbf{u}_p$ are orthogonal, so $\|\mathbf{u}_h \times \mathbf{u}_p\| = 1$. Let $\omega_x \equiv \boldsymbol{\omega} \cdot \left(\mathbf{u}_h \times \mathbf{u}_p\right)$ be the component of $\boldsymbol{\omega}$ orthogonal to both $\mathbf{u}_h$ and $\mathbf{u}_p$. (It is also orthogonal to $\mathbf{u}_n$.) This is the only component of $\boldsymbol{\omega}$ that has an effect on glint rate $\dot{\theta}$, so it can also be thought of as the observable component of $\boldsymbol{\omega}$. Also, $-\left\|\frac{^I d}{dt}\mathbf{u}_h\right\| \leq \left(\frac{^I d}{dt}\mathbf{u}_h\right) \cdot \mathbf{u}_p \leq \left\|\frac{^I d}{dt}\mathbf{u}_h\right\|$. The upper and lower bounds on $|\omega_x|$ are thus given by:

$$|\omega_x|_{\max} = |\dot{\theta}| + \left\|\frac{^I d}{dt}\mathbf{u}_h\right\| \tag{15a}$$

$$|\omega_x|_{\min} = \begin{cases} |\dot{\theta}| - \left\|\frac{^I d}{dt}\mathbf{u}_h\right\| & \text{if } |\dot{\theta}| > \left\|\frac{^I d}{dt}\mathbf{u}_h\right\| \\ 0 & \text{if } |\dot{\theta}| \leq \left\|\frac{^I d}{dt}\mathbf{u}_h\right\| \end{cases} \tag{15b}$$

The derivative norm $\left\|\frac{^I d}{dt}\mathbf{u}_h\right\|$ can be calculated using Eqs. (6)-(7). The glint rate $\dot{\theta}$ is estimated from the glint duration, as described in Section III.

III. Angular Velocity from Glint Duration

In the absence of attitude control, the time history of the angle $\theta(t)$ near a glint event is well-approximated by an hyperbola. (Even if attitude control is present, this is likely a good approximation in many cases.) The angle $\theta(t)$ between $\mathbf{u}_h$ and $\mathbf{u}_n$ tends to decrease at a relatively constant rate β until it nears the glint time t_g, transition smoothly through a minimum value of θ_g at t_g, and then increase at the same constant rate β. For a given set of surface properties, the angular width of glints is relatively constant. It can be specified by

the "edge angle" θ_e, such that glints occur for times such that $\theta(t) \leq \theta_e$. The times corresponding to the glint edges are t_{e1} and t_{e2}, and the overall glint width is $\Delta t = t_{e2} - t_{e1}$.

In cases without good attitude knowledge, the minimum angle θ_g is not known accurately. The true θ hyperbola for a given glint is one of a family of hyperbolae parameterized by the minimum angle θ_g, as illustrated in Fig. 2. For now, assume that θ_e and θ_g are known. This assumption will be addressed in

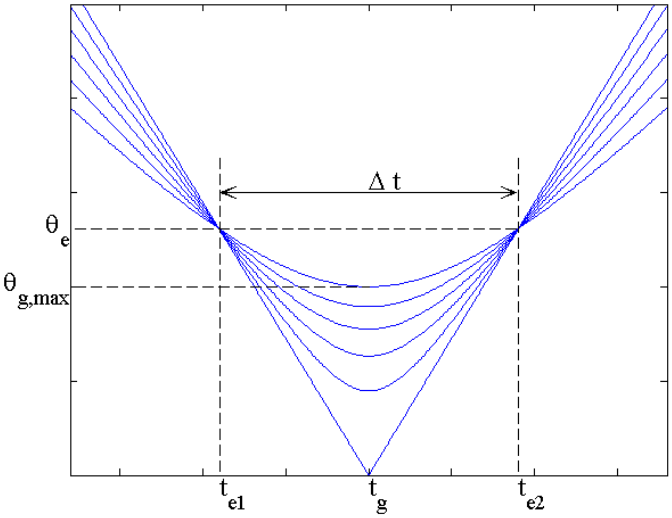

Figure 2. Family of hyperbolae for given θ_e and Δt

Section IV. The hyperbolic shape of $\theta(t)$ makes it possible to derive an expression for the derivative $\dot{\theta}$ in terms of θ_e, θ_g, and the glint width Δt.

The hyperbola $\theta(t)$ is described by

$$\frac{\theta^2(t)}{\theta_g^2} - \frac{(t - t_g)^2}{(\theta_g/\beta)^2} = 1 \tag{16}$$

or, in a more convenient form,

$$\theta^2(t) = \theta_g^2 + \beta^2 (t - t_g)^2 \tag{17}$$

One can derive an expression for the asymptotic slope β as a function of θ_e, θ_g, and the glint width Δt by substituting the point (t_e, θ_e) into Eq. (17) and solving for β^2:

$$\theta_e^2 = \theta_g^2 + \beta^2 (t_e - t_g)^2 \tag{18}$$

$$\beta^2 = \frac{\left(\theta_e^2 - \theta_g^2\right)}{(t_e - t_g)^2} \tag{19}$$

Assuming that $|t_{e1} - t_g| = |t_{e2} - t_g| = 0.5\Delta t$, the hyperbola is described by

$$\theta^2(t) = \theta_g^2 + \frac{4\left(\theta_e^2 - \theta_g^2\right)}{\Delta t^2} (t - t_g)^2 \tag{20}$$

The angular velocity bounds of Eq. (15) require the glint rate $\dot{\theta}$ at some given time t. One cannot use the time of maximum glint, t_g, for this purpose, because $\dot{\theta}$ goes to zero and Eq. (14) has a potential singularity (in the case where $\mathbf{u}_n = \mathbf{u}_h$, so that $\mathbf{u}_p$ is undefined). Instead, the glint edge times t_{e1} and t_{e2}, which are relatively easy to measure in a data set, are used. The glint rate $\dot{\theta}$ should have equal magnitudes at the two edges. Therefore, taking the derivative of Eq. (20) and solving for $\dot{\theta}$:

$$2\theta\dot{\theta} = \frac{8\left(\theta_e^2 - \theta_g^2\right)}{\Delta t^2} (t - t_g) \tag{21}$$

$$\dot{\theta} = \frac{4\left(\theta_e^2 - \theta_g^2\right)}{\theta \Delta t^2}\left(t - t_g\right) \tag{22}$$

Evaluating Eq. (22) at (t_e, θ_e) gives

$$\begin{aligned}\dot{\theta}\left(t_e\right) &= \frac{4\left(\theta_e^2 - \theta_g^2\right)}{\theta_e \Delta t^2}\left(t_e - t_g\right) \\ &= \frac{4\left(\theta_e^2 - \theta_g^2\right)}{\theta_e \Delta t^2}\frac{\Delta t}{2} \\ &= \frac{2\left(\theta_e^2 - \theta_g^2\right)}{\theta_e \Delta t} \\ &= \frac{2\theta_e}{\Delta t} - \frac{2\theta_g^2}{\theta_e \Delta t}\end{aligned} \tag{23}$$

For a given θ_e, θ_g, and measured Δt, Eq. (23) gives the value of $\dot{\theta}$ that can be substituted into the angular velocity bound equations.

IV. Implementation Issues

While Eqs. (15) and (23) for calculating angular velocity bounds from glint duration are simple, there are several difficulties that arise in implementation. First, it may be difficult to accurately measure the width of a glint event in a real data set with irregularly spaced observations, gaps, noise, etc.— especially if the glint is a shallow one. Second, the "edge angle" θ_e depends on the surface material properties of the reflecting object. Such properties may be known poorly, if at all. Finally, the "glint angle" θ_g (the smallest angle between $\mathbf{u}_n$ and $\mathbf{u}_h$ for a given glint event) cannot be determined accurately without knowing something about the object shape and attitude. Generally speaking, that information is not available in cases where the angular velocity is completely unknown.

A. Incorporating Uncertainty

One simple approach to the aforementioned issues is to incorporate all the existing sources of uncertainty directly into the angular velocity bounds. The form of Eq. (14) is such that only the component of $\boldsymbol{\omega}$ orthogonal to both $\mathbf{u}_h$ and $\mathbf{u}_n$ is at all observable from glint rate, and only upper and lower bounds on that component are possible without attitude knowledge. Suppose that the quantities Δt, θ_e, and θ_g are also known only to lie within some range: $\Delta t_{\min} \leq \Delta t \leq \Delta t_{\max}$, $\theta_{e,\min} \leq \theta_e \leq \theta_{e,\max}$, and $\theta_{g,\min} \leq \theta_g \leq \theta_{g,\max}$. Then the bounding values can be used in Eqs. (15) and (23) as necessary to create the most conservative upper and lower bounds.

First, one must take this approach with Eq. (23) to find minimum and maximum values of $\dot{\theta}\left(t_e\right)$:

$$\dot{\theta}_{\min}\left(t_e\right) = \frac{2\theta_{e,\min}}{\Delta t_{\max}} - \frac{\theta_{g,\max}^2}{\theta_{e,\min}\Delta t_{\max}} \tag{24a}$$

$$\dot{\theta}_{\max}\left(t_e\right) = \frac{2\theta_{e,\max}}{\Delta t_{\min}} - \frac{\theta_{g,\min}^2}{\theta_{e,\max}\Delta t_{\min}} = \frac{2\theta_{e,\max}}{\Delta t_{\min}} \tag{24b}$$

The final simplification in Eq. (24b) recognizes that the minimum possible value of θ_g is zero; this occurs for the case of a full glint. When applying Eq. (24a), one must take care to use a consistent pair of values for $\theta_{e,\min}$ and $\theta_{g,\max}$: For a given glint, $\theta_e > \theta_g$ because θ_g is by definition the minimum θ achieved during the glint. In fact, θ_g must be sufficiently less than θ_e in order for any glint to be visible in the data.

Once $\dot{\theta}_{\min}\left(t_e\right)$ and $\dot{\theta}_{\max}\left(t_e\right)$ have been calculated, these values can be used within the conservative version of Eqs. (15a) and (15b):

$$|\omega_x|_{\max} = |\dot{\theta}_{\max}| + \left\| \frac{{}^I d}{dt}\mathbf{u}_h \right\| \tag{25a}$$

$$|\omega_x|_{\min} = \begin{cases} |\dot{\theta}_{\min}| - \left\| \frac{{}^I d}{dt}\mathbf{u}_h \right\| & \text{if } |\dot{\theta}_{\min}| > \left\| \frac{{}^I d}{dt}\mathbf{u}_h \right\| \\ 0 & \text{if } |\dot{\theta}_{\min}| \leq \left\| \frac{{}^I d}{dt}\mathbf{u}_h \right\| \end{cases} \tag{25b}$$

B. Selecting θ_e and θ_g

The uncertainty associated with Δt is largely determined by the quality of available data, and it is not difficult to select reasonable bounds for this quantity. Even with the conservative bounds described in Section A, it is necessary to have a reasonable starting point for the angles θ_e and θ_g if such values are not provided. As described in the previous subsection, the choice of θ_e and θ_g cannot be completely independent. The following discussion is not intended to be the final word on this subject, but it should provide some useful guidelines.

Glints occur when one of an object's facet normal vectors $\mathbf{u}_n$ gets close enough to the specular direction $\mathbf{u}_h$ that bright specular reflection dominates diffuse reflection. The range of angles within which this occurs is known as the *specular lobe*, and the size of the specular lobe depends on the surface material and surface finish associated with that facet. The more shiny and mirror-like a facet is, the smaller the size of the specular lobe, and vice versa. The threshold angle for specular reflection is defined in this document as the glint edge angle θ_e.

If one knows the reflecting object to be very shiny, a small value of θ_e can be used, and a large value can be selected if the reflecting object is less mirror-like. In practice, it may be necessary to use a relatively small $\theta_{e,\min}$ and a relatively large $\theta_{e,\max}$ to account for uncertainty (and in such cases, the angular velocity bounds will not be tight). If many deep, distinct glints are observed in the data, it is likely that θ_e is small. Conversely, the presence of only shallower, less-distinct glints suggests a larger value of θ_e.

For a given BRDF model, one can use simulations to empirically determine the typical values of θ_e for a particular set of surface parameters. One such model is the Ashikhmin-Shirley BRDF model.[13] Note that although this model allows for anisotropic reflection, this paper's discussion assumes isotropy. This assumption is enforced by setting the parameters n_u and n_v equal; the resulting single parameter is herein called n_{uv}. In Ashikhmin's model, the size of the specular lobe is controlled primarily by a single expression in the numerator: $(\mathbf{u}_h \cdot \mathbf{u}_n)^{n_{uv}}$.

Under the assumption of a relatively shiny facet with $n_{uv} = 1000$, the angle θ_e has been found in simulations to be roughly 0.13048 radians (7.476°). This value is fairly consistent over multiple simulations and observed glints, varying by roughly 1° at most. Rather than running new simulations and deriving an empirical θ_e for each possible n_{uv}, a scaling procedure is recommended. One would expect the glint threshold to occur for roughly the same value of $(\mathbf{u}_h \cdot \mathbf{u}_n)^{n_{uv}}$, regardless of the specific n_{uv}. This expression can be rewritten as $(\cos\theta)^{n_{uv}}$. Let $\theta_{e0} = 0.13048$ radians and $n_{uv0} = 1000$ be "reference values". Then

$$\begin{aligned} (\cos\theta_e)^{n_{uv}} &= (\cos\theta_{e0})^{n_{uv0}} \\ \cos\theta_e &= (\cos\theta_{e0})^{\frac{n_{uv0}}{n_{uv}}} \\ \theta_e &= \cos^{-1}\left[(\cos\theta_{e0})^{\frac{n_{uv0}}{n_{uv}}}\right] \end{aligned} \tag{26}$$

Additional simulations for several different values of n_{uv} such as 500 or 100 have indicated that this scaling procedure is fairly successful at predicting the values of θ at the glint edges. The observed errors have been similar to the level of variation seen in the simulations themselves. It is further conceivable that a similar scaling procedure might be derived for a different BRDF model, provided one could isolate the terms responsible for the size of the specular lobe.

Once upper and lower bounds for θ_e have been selected, one can consider θ_g. As previously mentioned, the minimum possible value of θ_g is zero; this occurs during a full glint, when $\mathbf{u}_n$ and $\mathbf{u}_h$ align perfectly. For purposes of Eq. (24a), the maximum value is required—this value corresponds to a very shallow glint. In order for any distinct glint to be visible in a light curve, θ_e must exceed θ_g by some minimum, non-negligible amount.

In simulations using the Ashikhmin-Shirley BRDF model, the shallowest distinctly recognizable glints for a given n_{uv} were sought. For the $n_{uv} = 1000$ case, such shallow glints were found to have a glint angle of roughly $\theta_g = 0.10588$ radians (6.066°), or about 1.5° less than θ_e. As θ_e becomes larger, however, the difference between θ_e and θ_g required to produce a clear glint also becomes larger. One reasonably successful approach is to reprise the scaling procedure introduced for θ_e:

$$\theta_g = \cos^{-1}\left[(\cos\theta_{g0})^{\frac{n_{uv0}}{n_{uv}}}\right] \tag{27}$$

where $\theta_{g0} = 0.10588$ radians and $n_{uv0} = 1000$ can be used as reference values.

V. Results

The glint duration techniques described in the preceding sections were applied in several contexts: to simulated light curves, data from a laboratory experiment, and data from the Galaxy 15 communications satellite.

A. Results from Simulated Data

A number of truth model simulations were performed in order to determine reasonable rules of thumb for selecting θ_e and θ_g. This subsection describes the results of one representative simulation in detail.

For the simulated scenario, the reflecting object is a shiny rectangular prism (with BRDF parameters $R_{\text{spec}} = 0.7, R_{\text{diff}} = 0.3$, and $n_{uv} = 1000$). The object's orbit is near, but not exactly, geostationary, and it tumbles with an average angular rate of 3.8×10^{-3} radians/second. One distinct glint was observed in the light curve during the first 10 minutes of simulated time, as shown in Fig. 3. The glint duration Δt

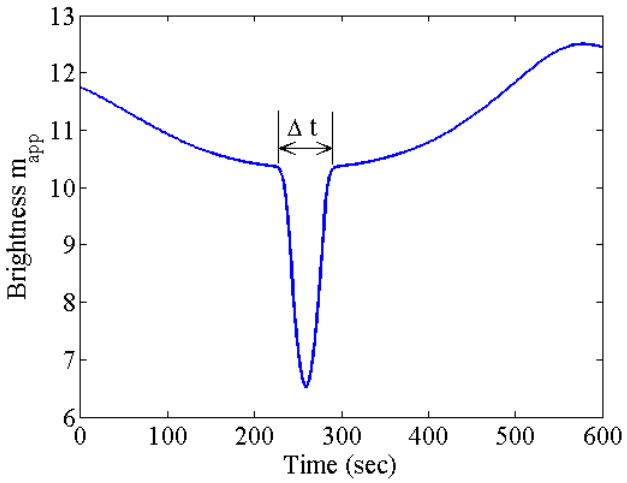

Figure 3. Simulated light curve with glint

was roughly 62 seconds. Assuming that the parameter $n_{uv} = 1000$ is fairly well-known for this case, 0.1305 radians was selected as the glint edge angle θ_e (with no uncertainty), and 0.1059 radians was selected as the maximum glint angle $\theta_{g,\max}$. The minimum and maximum glint widths were chosen as $\Delta t_{\min} = 58$ seconds and $\Delta t_{\max} = 66$ seconds.

Application of Eqs. (24a) and (24b) gives the minimum and maximum glint rates $\dot{\theta}_{\min} = 1.35 \times 10^{-3}$ rad/sec and $\dot{\theta}_{\max} = 4.50 \times 10^{-3}$ rad/sec. These values are in turn used to evaluate Eqs. (25a) and (25b). The magnitude of $\| \frac{^I d}{dt} \mathbf{u}_h \|$, the inertial derivative of $\mathbf{u}_h$, was found to be approximately 3.66×10^{-5}, so the bounds on the observable component of $\boldsymbol{\omega}$ are $|\omega_x|_{\min} = 1.31 \times 10^{-3}$ rad/sec and $|\omega_x|_{\max} = 4.54 \times 10^{-3}$ rad/sec. For comparison, the true (simulated) value of the observable component of $\boldsymbol{\omega}$ at the glint edges was found to be 3.57×10^{-3} rad/sec, which lies well within the computed bounds. In this particular example, the overall angular velocity magnitude also falls within the bounds, but that is not always the case. The angular velocity results are summarized in Table 1.

Table 1. Summary of results for simulated light curve

Δt	62 sec
$\lvert\omega_x\rvert_{\min}$	1.31×10^{-3} rad/sec
$\lvert\omega_x\rvert_{\max}$	4.54×10^{-3} rad/sec
$\lvert\omega_x\rvert_{\text{true}}$	3.57×10^{-3} rad/sec
$\lVert\boldsymbol{\omega}\rVert_{\text{true}}$	3.80×10^{-3} rad/sec

B. Results from Experimental Data

A series of laboratory experiments were conducted to create synthetic light curves for some well-characterized test objects. In each experiment, a light source was focused on the test object, which rotated on a turntable. Other sources of light and reflection were eliminated. A series of images was collected by a camera, and the light curve was constructed by calculating the total brightness in the image pixels at each time step. The size and shape of the test objects, and locations of the object, camera, and light source, were found by measuring.

One of the test objects which exhibited distinct specular glints was a flat, relatively shiny piece of sheet metal. The corresponding light curve is shown in Fig. 4. As the light source, object, and camera were all

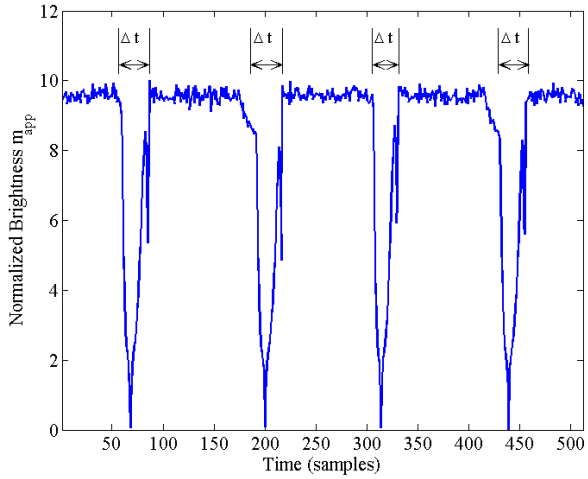

Figure 4. Experimental light curve with multiple glints

at fixed locations, the glint angle $\mathbf{u}_h$ was constant and its derivative was zero in the inertial frame. The average glint duration over the data set was $\Delta t = 29.25$ samples. (The camera sampling interval was used for the time units.) It was possible to calculate the glint edge angles θ_e from the known configuration and object rotation angles: On average they were about $\theta_e = 0.416$ radians (23.8°). Using the scaling procedure in Eq. (26), this corresponds to a parameter of $n_{uv} = 95.87$. For this n_{uv}, Eq. (27) suggests $\theta_{g,\max} = 0.339$ radians (19.42°). The actual average θ_g for this experiment was 0.201 radians (11.51°), so the estimated $\theta_{g,\max}$ is quite conservative. A glint duration uncertainty of ±2 samples was assumed.

The glint rate bounds were found from Eq. (24) to be $8.96 \times 10^{-3} \leq \dot{\theta}\,(t_e) \leq 3.07 \times 10^{-2}$ rad/sample. As $\|\frac{{}^I d}{dt}\mathbf{u}_h\| = 0$ for this case, the bounds on the observable component of angular velocity were exactly the bounds on $\dot{\theta}$: $8.96 \times 10^{-3} \leq |\omega_x\,(t_e)\,| \leq 3.07 \times 10^{-2}$ rad/sample. The true magnitude of the observable component of $\boldsymbol{\omega}$ was $|\omega_x| = 2.19 \times 10^{-2}$ rad/sample, and the magnitude of the overall rotation rate was $\|\boldsymbol{\omega}\| = 2.55 \times 10^{-2}$ rad/sample. Table 2 summarizes these results.

Table 2. Summary of results for experimental light curve

Δt	29.25 samp
$\|\omega_x\|_{\min}$	8.96×10^{-3} rad/samp
$\|\omega_x\|_{\max}$	3.07×10^{-2} rad/samp
$\|\omega_x\|_{\text{true}}$	2.19×10^{-2} rad/samp
$\|\boldsymbol{\omega}\|_{\text{true}}$	2.55×10^{-2} rad/samp

C. Results from Galaxy 15 Data

The glint duration algorithms were also applied to real light curve data from the Galaxy 15 communications satellite. Galaxy 15 is nominally geostationary and nadir-pointing, but no detailed shape model or attitude

history were ever provided, so it was not possible to compute "true" values of the angle θ or related quantities. The nominal angular velocity for the nadir-pointing configuration was computed. Surface reflection parameters were not given.

The light curve exhibited a dominant deep "V" shape of increased brightness due to the relative motion of the Sun, but it was not possible to clearly identify a specular glint within this region. In addition, however, there were five smaller distinct glints, as indicated in Fig. 5. The average duration of these glints was about 550.5 seconds, and the corresponding bounds were computed. The results presented here are the averages over the five glint events.

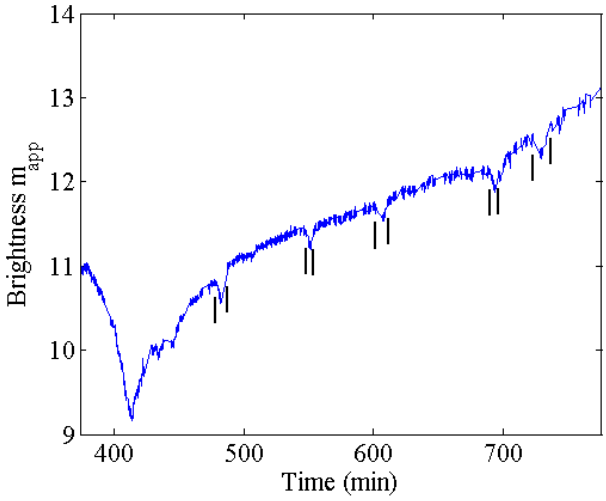

Figure 5. Galaxy 15 light curve with small glints

The angular velocity bounds were computed under several different assumptions for the reflection parameter n_{uv}. Large values of n_{uv} (more mirror-like reflection) give conservative lower bound estimates for $|\omega_x|$, and smaller values of n_{uv} give conservative upper bound estimates. Assuming $n_{uv} = 1000$, the lower bound on the observable part of $\boldsymbol{\omega}$ is $|\omega_x|_{\min} = 1.24 \times 10^{-4}$ rad/sec. Of course, this is also a lower bound on the magnitude of the overall vector $\boldsymbol{\omega}$. For an assumption of $n_{uv} = 100$, the computed upper bound was $|\omega_x|_{\max} = 1.84 \times 10^{-3}$ rad/sec. In comparison, the magnitude of the nominal angular velocity for the geostationary, nadir-pointing configuration is $\|\boldsymbol{\omega}\|_{\text{nom}} = 7.29 \times 10^{-5}$ rad/sec. These results are summarized in Table 3.

Table 3. Summary of results for Galaxy 15 light curve

Δt	550.5 sec
$\|\omega_x\|_{\min}$	1.244×10^{-4} rad/sec
$\|\omega_x\|_{\max}$	1.840×10^{-3} rad/sec
$\|\boldsymbol{\omega}\|_{\text{nom}}$	7.290×10^{-5} rad/sec

Note that the nominal angular velocity magnitude is about half that of the conservative lower bound calculated from the glint widths. There are several possible explanations for this discrepancy. The most obvious conclusion is that the observed glints are caused by some form of attitude maneuvers - such as periodic solar panel rotations intended to keep the solar panels in an approximately sun-pointing configuration. Before accepting that hypothesis, it is wise to look at previous analyses of the Galaxy 15 light curve.[14,15] Reference 15, in particular, examines these "faint glints" in depth, and concludes that the shift in glint epoch time from day to day is consistent with glints from components mounted on the main bus, rather than the solar panels. As shown here, the duration of the glints strongly suggests that these components are moving. Alternatively, the glinting components may not conform to the theoretical glint width because they fail to satisfy the "flat facet" assumption and are in fact cylindrical or more complex in shape.

This case indicates the power of the proposed analysis: While it cannot determine angular velocity in

any exact sense, measurements of glint width can be used to identify non-nominal behavior or changes in behavior, even when details like attitude and shape are poorly known.

VI. Conclusions

In this paper, a technique was developed that constrains the magnitude of SO angular velocity based on the time duration of specular glint events. The algorithm derives a set of equations that relate the observable part of the sidereal angular rate to the derivative of the angle between the phase angle bisector and the normal vector of the reflecting facet. An additional derivation relates this derivative to the observed glint width. Uncertainties in the form of upper and lower bounds on measured or assumed quantities can be easily incorporated. This paper's method is applied to data from three sources: simulations, laboratory experiments, and a real satellite. The computed bounds successfully bracketed the observable component of angular velocity in all cases for which the "truth" was available for comparison, although in many cases the bounds were not very tight. However, even such limited rate information may be useful in detecting anomalous rate behavior, or in selecting a reasonable initial rate estimate for a Kalman filter.

References

[1]Jah, M. and Madler, R., "Satellite Characterization: Angles and Light Curve Data Fusion for Spacecraft State and Parameter Estimation," *Proceedings of the Advanced Maui Optical and Space Surveillance Technologies Conference*, Vol. 49, Sept. 2007, Maui, HI.

[2]Linares, R., Shoemaker, M., Walker, A., Mehta, P. M., Palmer, D. M., Thompson, D. C., Koller, J., and Crassidis, J. L., "Photometric Data from Non-Resolved Objects for Space Object Characterization and Improved Atmospheric Modeling," *Advanced Maui Optical and Space Surveillance Technologies Conference*, Sept. 2013, Maui, HI.

[3]Linares, R., Jah, M. K., Crassidis, J. L., and Nebelecky, C. K., "Space Object Shape Characterization and Tracking Using Light Curve and Angles Data," *J. of Guidance, Control, and Dynamics*, Vol. 37, No. 1, 2014, pp. 13–25.

[4]Wetterer, C. J., Hunt, B., Kervin, P., and Jah, M., "Comparison of Unscented Kalman Filter and Unscented Schmidt Kalman Filter in Predicting Attitude and Associated Uncertainty of a Geosynchronous Satellite," *Advanced Maui Optical and Space Surveillance Technologies Conference*, Sept. 2014, Maui, HI.

[5]Alcala, C. M. and Brown, J. H., "Space Object Characterization Using Time-Frequency Analysis of Multi-Spectral Measurements from the Magdalena Ridge Observatory," *Advanced Maui Optical and Space Surveillance Technologies Conference*, Sept. 2009, Maui, HI.

[6]Papushev, P., Karavaev, Y., and Mishina, M., "Investigations of the Evolution of Optical Characteristics and Dynamics of Proper Rotation of Uncontrolled Geostationary Artificial Satellites," *Adv. in Space Research*, Vol. 43, No. 9, 2009.

[7]Hall, D., Africano, J., Archambeault, D., Birge, B., Witte, D., and Kervin, P., "AMOS Observations of NASA's IMAGE Satellite," *Advanced Maui Optical and Space Surveillance Technologies Conference*, Sept. 2006, Maui, HI.

[8]Binz, C. R., Davis, M. A., Kelm, B. E., and Moore, C. I., "Optical Survey of the Tumble Rates of Retired GEO Satellites," *Advanced Maui Optical and Space Surveillance Technologies Conference*, Sept. 2014, Maui, HI.

[9]Cognion, R. L., "Rotation Rates of Inactive Satellites Near Geosynchronous Orbit," *Advanced Maui Optical and Space Surveillance Technologies Conference*, Sept. 2014, Maui, HI.

[10]Wallace, B., Somers, P., and Scott, R., "Determination of Spin Axis Orientation of Geosynchronous Objects Using Space-Based Sensors: An Initial Feasibility Investigation," *Advanced Maui Optical and Space Surveillance Technologies Conference*, Sept. 2010, Maui, HI.

[11]Somers, P., "Cylindrical RSO Signatures, Spin Axis Orientation and Rotation Period Determination," *Advanced Maui Optical and Space Surveillance Technologies Conference*, Sept. 2011, Maui, HI.

[12]Vrba, F. J., DiVittorio, M. E., Hindsley, R. B., Schmitt, H. R., Armstrong, J. T., Shankland, P. D., Hutter, D. J., and Benson, J. A., "A Survey of Geosynchronous Satellite Glints," *Advanced Maui Optical and Space Surveillance Technologies Conference*, Sept. 2009, Maui, HI.

[13]Ashikhmin, M. and Shirley, P., "An Anisotropic Phong Light Reflection Model," Tech. Rep. UUCS-00-014, University of Utah, Salt Lake City, UT, 2000.

[14]Hall, D., "AMOS Galaxy 15 Satellite Observations and Analysis," *Advanced Maui Optical and Space Surveillance Technologies Conference*, Sept. 2011, Maui, HI.

[15]Hall, D. and Kervin, P., "Analysis of Faint Glints from Stabilized GEO Satellites," *Advanced Maui Optical and Space Surveillance Technologies Conference*, Sept. 2013, Maui, HI.